1-1-2023

Keck spectroscopy of the coma cluster ultra-diffuse galaxy Y358: dynamical mass in a wider context

Jonah S. Gannon
Swinburne University of Technology

Duncan A. Forbes
Swinburne University of Technology

Jean P. Brodie
Swinburne University of Technology

Aaron J. Romanowsky
San Jose State University, aaron.romanowsky@sjsu.edu

Warrick J. Couch
Swinburne University of Technology

See next page for additional authors

Recommended Citation

Jonah S. Gannon, Duncan A. Forbes, Jean P. Brodie, Aaron J. Romanowsky, Warrick J. Couch, and Anna Ferré-Mateu. "Keck spectroscopy of the coma cluster ultra-diffuse galaxy Y358: dynamical mass in a wider context" *Monthly Notices of the Royal Astronomical Society* (2023): 3653-3666. https://doi.org/10.1093/mnras/stac3264

Monthly Notices of the ROYAL ASTRONOMICAL SOCIETY

MNRAS **518,** 3653–3666 (2023) https://doi.org/10.1093/mnras/stac3264
Advance Access publication 2022 November 11

Keck spectroscopy of the coma cluster ultra-diffuse galaxy Y358: dynamical mass in a wider context

Jonah S. Gannon [1]★ Duncan A. Forbes,[1] Jean P. Brodie,[1,2] Aaron J. Romanowsky [2,3] Warrick J. Couch[1] and Anna Ferré-Mateu [4,5]

[1] *Centre for Astrophysics and Supercomputing, Swinburne University, John Street, Hawthorn VIC 3122, Australia*
[2] *University of California Observatories, 1156 High Street, Santa Cruz, CA 95064, USA*
[3] *Department of Physics and Astronomy, San José State University, One Washington Square, San Jose, CA 95192, USA*
[4] *Instituto de Astrofísica de Canarias, Calle Vía Láctea S/N, E-38205 La Laguna, Tenerife, Spain*
[5] *Departamento de Astrofísica, Universidad de La Laguna, E-38206 La Laguna (S.C. Tenerife), Spain*

Accepted 2022 November 7. Received 2022 November 7; in original form 2022 June 8

ABSTRACT

We examine ultra-diffuse galaxies (UDGs) and their relation to non-UDGs in mass–radius–luminosity space. We begin by publishing Keck/KCWI spectroscopy for the Coma cluster UDG Y358, for which we measure both a recessional velocity and velocity dispersion. Our recessional velocity confirms association with the Coma cluster and Y358's status as a UDG. From our velocity dispersion (19 ± 3 km s^{-1}), we calculate a dynamical mass within the half-light radius, which provides evidence for a core in Y358's dark matter halo. We compare this dynamical mass, along with those for globular cluster (GC)-rich/-poor UDGs in the literature, to mass profiles for isolated, gas-rich UDGs, and UDGs in the NIHAO/FIRE simulations. We find GC-poor UDGs have dynamical masses similar to isolated, gas-rich UDGs, suggesting an evolutionary pathway may exist between the two. Conversely, GC-rich UDGs have dynamical masses too massive to be easily explained as the evolution of the isolated, gas-rich UDGs. The simulated UDGs match the dynamical masses of the GC-rich UDGs. However, once compared in stellar mass–halo mass space, the FIRE/NIHAO-simulated UDGs do not match the halo masses of either the isolated, gas-rich UDGs or the GC-rich UDGs at the same stellar mass. Finally, we supplement our data for Y358 with other UDGs that have measured velocity dispersions in the literature. We compare this sample to a wide range of non-UDGs in mass–radius–luminosity space, finding UDGs have a similar locus to non-UDGs of similar luminosity with the primary difference being their larger half-light radii.

Key words: galaxies: elliptical and lenticular, cD – galaxies: formation – galaxies: fundamental parameters – galaxies: haloes – galaxies: kinematics and dynamics.

1 INTRODUCTION

The class of 'ultra-diffuse galaxy' (UDG) was first coined by van Dokkum et al. (2015) in relation to a subset of large half-light radius, low surface brightness galaxies in the Coma cluster. Formally, they classified UDGs as galaxies with half-light radius, $R_e > 1.5$ kpc, and central surface brightness, $\mu_{0,g} > 24$ mag arcsec^{-2}. Galaxies fitting this definition have been discovered in a wide range of environments both before (e.g. Disney 1976; Sandage & Binggeli 1984; Bothun et al. 1987; Impey, Bothun & Malin 1988; Dalcanton et al. 1997; Impey & Bothun 1997) and after 2015 (e.g. Yagi et al. 2016; Martínez-Delgado et al. 2016; Janssens et al. 2017, 2019; van der Burg et al. 2017; Román & Trujillo 2017b, a; Müller, Jerjen & Binggeli 2018; Forbes et al. 2019, 2020b; Prole et al. 2019b; Román et al. 2019; Barbosa et al. 2020; Zaritsky et al. 2019, 2021, La Marca et al. 2022).

It is worth noting that since their coining by van Dokkum et al. (2015), many other authors have applied the same UDG term to galaxies fitting a different criteria set. For example, in the catalogue of Yagi et al. (2016), the UDG size criterion was relaxed to $R_e > 0.7$ kpc. Other authors have used a surface brightness criterion based on the average surface brightness within the half-light radius ($\langle\mu\rangle_e$; e.g. van der Burg et al. 2017; Janssens et al. 2017, 2019; Gannon et al. 2022), or altered the surface brightness/filter band at which it applies (e.g. Janssens et al. 2017, 2019; Forbes et al. 2020b). The studies of Ruiz-Lara et al. (2018) and Chilingarian et al. (2019) went further, applying the UDG term to a set of galaxies that are generally brighter and smaller than the original definition. Using the ROMULUS simulations, Van Nest et al. (2022) found that the choice of UDG criteria is key, having a large impact on the implied mechanisms underpinning their formation. Specifically, definitions for what comprises a 'UDG' that are less restrictive may dilute the link between objects fitting the definition and their underlying formation mechanism.

For UDGs, their necessarily faint nature means spectroscopy of their stellar body requires a large time investment on 8m + class telescopes. While gas-rich UDGs can be studied using their gas-kinematics (e.g. Mancera Piña et al. 2019, 2022; Kong et al.

★ E-mail: jonah.gannon@gmail.com

2022), this method is not available for quiescent UDGs. As such, spectroscopy has largely focused on deriving the properties of single, or a small handful of, UDGs (e.g. van Dokkum et al. (e.g. van Dokkum et al. 2017; Alabi et al. 2018; Ferré-Mateu et al. 2018; Toloba et al. 2018; Danieli et al. 2019; Emsellem et al. 2019; Martín-Navarro et al. 2019; van Dokkum et al. 2019; Gannon et al. 2020, 2021, 2022; Müller et al. 2020; Forbes et al. 2021). Many of these UDGs have been targeted because of their extreme properties, even within the UDG class. For example, many UDGs have received targeted spectroscopy due to their anomalously populous globular cluster (GC) systems (e.g. Dragonfly 44 and DFX1 van Dokkum et al. 2017, 2019), a known indicator of a massive dark matter halo (Spitler & Forbes 2009; Harris, Blakeslee & Harris 2017; Forbes et al. 2018; Burkert & Forbes 2020; Zaritsky 2022). While this has led to a slew of interesting discoveries, it has likely resulted in an overall literature that is poorly representative of the UDG population as a whole.

Simulations of galaxy formation primarily propose that UDGs form in a 'puffy dwarf' scenario. In brief, they suggest UDGs are simply an extension of the regular dwarf galaxy population to larger sizes. The primary cause of this puffing up is usually attributed to higher than average halo spin (Amorisco & Loeb 2016; Rong et al. 2017; Liao et al. 2019), strong stellar feedback (Di Cintio et al. 2017; Chan et al. 2018), tidal forces/quenching (Carleton et al. 2019; Sales et al. 2020; Tremmel et al. 2020), early mergers (Wright et al. 2021), or combinations of the aforementioned four (Jiang et al. 2019; Liao et al. 2019; Martin et al. 2019). It seems likely that these scenarios account for many, perhaps even most, galaxies residing in the UDG definition.

Early work incorporating GCs into simulations of 'puffy dwarf' UDG formation suggested the formation of GC-rich UDGs may be possible in dwarf-like dark matter haloes (Carleton et al. 2021). However, this formation scenario cannot explain known GC–dark matter halo mass scaling relations and is unable to produce GC-rich UDGs in massive dark matter haloes (Gannon et al. 2022).

Alternatively, it has been suggested that GC-rich, massive halo UDGs may be the dark matter-dominated remnants of the earliest phases of galaxy formation. The observational expectation is for the galaxy to have quenched early and catastrophically. In doing so, it fails to form a large portion of its expected stellar mass (Peng & Lim 2016; van Dokkum et al. 2016; Buzzo et al. 2022; Danieli et al. 2022; Janssens et al. 2022; Villaume et al. 2022). These massive halo UDGs are not reproduced by leading cosmological simulations of galaxy formation. We note the work of Saifollahi et al. (2021, 2022), which suggested the rich GC systems of five previously studied Coma cluster UDGs may be the result of measurement error. However, even after their measurement corrections, Saifollahi et al. (2022) concluded an early formation and quenching scenario is still one of the most viable formation pathways. Saifollahi et al. (2022) referred to this UDG formation process as a 'failed dwarf galaxy' scenario. Furthermore, follow-up spectroscopy, which allows measurement of a dynamical mass, largely supports the idea that GC-rich UDGs may reside in massive dark matter haloes (van Dokkum et al. 2019; Gannon et al. 2020, 2022; Forbes et al. 2021). It is not currently clear what fraction of the population massive halo UDGs represent.

For pressure-supported systems, it has been well established that in velocity dispersion, effective radius, and surface brightness space, galaxies reside on a so-called 'fundamental plane' (Djorgovski & Davis 1987; Dressler 1987; Faber et al. 1987). The fundamental plane offers unique insights into the physical processes, generating pressure-supported systems and thus constrains their formation (e.g. Borriello, Salucci & Danese 2003; Cappellari et al. 2006; Forbes et al. 2008; Graves & Faber 2010; Tollerud et al. 2011; Zaritsky et al. 2019). The fundamental plane and altered forms of it, such as mass–radius–luminosty space (Tollerud et al. 2011) or the fundamental manifold (Zaritsky, Gonzalez & Zabludoff 2006), have been shown to extend over nearly eight orders of magnitude in luminosity. These offer a connection from the dwarf spheroidals to giant elliptical galaxies (Zaritsky et al. 2006; Forbes et al. 2008; Tollerud et al. 2011). This allows an exploration of the relationship between luminous matter and dark matter haloes from the smallest to the largest structures in the Universe. It is also critical to our understanding of the dominant galaxy formation processes on different mass scales. With detailed studies of mass profiles being prohibitively time intensive and still leaving great uncertainty in total UDG halo masses (van Dokkum et al. 2019), placing large samples of UDGs on these relations is key to understanding their formation (cf. Gannon et al. 2022). We adopt the latter approach in this work.

Here, we present new Keck II/Keck Cosmic Web Imager (KCWI) spectroscopy for the Coma cluster UDG Y358. From these data, we measure both a recessional velocity and a velocity dispersion (Section 2). From our velocity dispersion, we measure a dynamical mass. We compare this dynamical mass to dark matter mass profiles to look for evidence of a core or cusp (Section 3). We additionally compare Y358's dynamical mass, along with dynamical masses for other UDGs, to mass profiles of isolated, gas-rich UDGs along with those from the NIHAO and FIRE simulations (Section 3.2). To contextualize this comparison, we compare the UDGs, both observed and simulated, in stellar mass–halo mass space (Section 3.3). We then supplement our Y358 data with those for literature UDGs with the intention of placing all on the fundamental plane (Section 4). In Section 4.1, we discuss the biases present in our sample. In Section 5, we place UDGs in mass–radius–luminosity space, discussing their location on the plane in the context of UDG formation compared to non-UDGs on the plane. We present the concluding remarks of our study in Section 6. The literature sample discussed in Sections 4 & 5 is presented in Appendix A.

2 NEW KECK COSMIC WEB IMAGER DATA

Here, we present new KCWI data for the UDG, Y358. We target this galaxy due to its rich GC system, which is indicative of a massive dark matter halo. Using the GC counts for Y358 from Lim et al. (2018; $N_{\rm GC} = 28.0 \pm 5.3$) and the $N_{\rm GC}$–halo mass relationship of Burkert & Forbes (2020), we infer a total dark matter halo mass of $(1.4 \pm 0.25) \times 10^{11}\,{\rm M}_{\odot}$ for Y358. The Lim et al. (2018) GC number is between the richness found by van Dokkum et al. (2017, 45 ± 14) and the 90 per cent upper limit from Amorisco et al. (2018, 18.4) for Y358. This is also the number used in the study of Forbes et al. (2020a) for Y358. Based on this GC richness, Y358 is expected to have a dark matter halo $>1\sigma$ more massive than expected given its stellar mass ($M_{\star} = 1.38 \times 10^{8}\,{\rm M}_{\odot}$; Forbes et al. 2020a).

The integral field spectroscopy for the UDG Y358 was observed using KCWI (Morrissey et al. 2018) on 2020, March 21 (Program: U191; PI: Brodie). Skies were dark and clear with 1.2' seeing. KCWI was configured using the medium slicer and 'BH3' grating with a central wavelength of 5170 Å (R $\approx$ 9900; $\sigma_{\rm inst} \approx 13\,{\rm km\,s^{-1}}$). We display a *Hubble Space Telescope* (*HST*) image of the galaxy, along with the KCWI pointing in Fig. 1.

The data were reduced using the standard KCWI data reduction pipeline along with the extra post-pipeline trimming and flat-fielding steps described in Gannon et al. (2020). Spectra were extracted from the reduced data cubes using a 7 by 13 spaxel box centred on the galaxy with offset regions of the slicer as subtracted sky. These

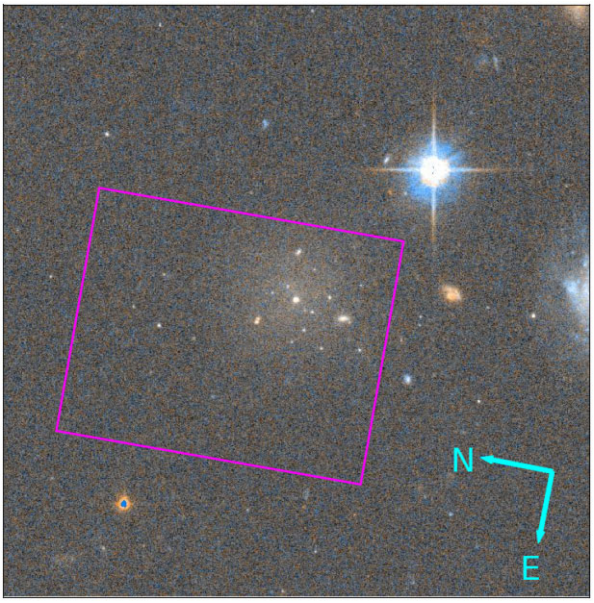

Figure 1. A 0.6' × 0.6' (17.5 × 17.5 kpc at Coma Cluster distance), two colour (F814W/F475W) *HST* cutout centred on Y358. The magenta rectangle indicates the positioning of the KCWI field of view. North and East are as indicated (cyan arrows). Of note are the numerous compact sources that appear associated with Y358, suggesting it likely hosts a rich GC system (Lim et al. 2018). A central compact source suggests it is nucleated.

spectra were then barycentric corrected (Tollerud 2015) and median combined. The resulting spectrum has S/N of 11 Å^{-1} with a total exposure time of 26 400 s. This spectrum has a wavelength range of 4923–5393 Å.

We fitted the spectrum using `pPXF` (Cappellari 2017) and the Coelho (2014) library with 241 different combinations of input parameters as per previous work (i.e. Gannon et al. 2020, 2021, 2022). We display a smoothed version of our final spectrum, along with an example fit and fit residuals, in Fig. 2. Our final values for the recessional velocity (7969 ± 2 km s^{-1}) and the velocity dispersion (19 ± 3 km s^{-1}) were taken from the median of these fits. We consistency checked these by fitting the red and blue halves of the spectrum. We also fitted the entire spectrum using a KCWI observation of the Milky Way GC Messier 3 as a template. These consistency checks were all within the uncertainties for our quoted values for both recessional velocity and velocity dispersion.

For the imaging properties of Y358, we use the values reported in table 1 of van Dokkum et al. (2017). We summarize the properties of Y358 in Table A1. Our recessional velocity for Y358 confirms its association with the Coma cluster. Combining this confirmation with the van Dokkum et al. (2017) imaging, we are able to confirm its status as a UDG.

3 RESULTS

We measure a dynamical mass for Y358 within the 3D de-projected half-light radius ($R_{1/2}$) using the mass estimator of Wolf et al. (2010). Using the 2D projected, circularized half-light radius ($R_{e,\,\mathrm{circ}}$) and the luminosity-weighted line-of-sight velocity dispersion within this radius (σ), it takes the form:

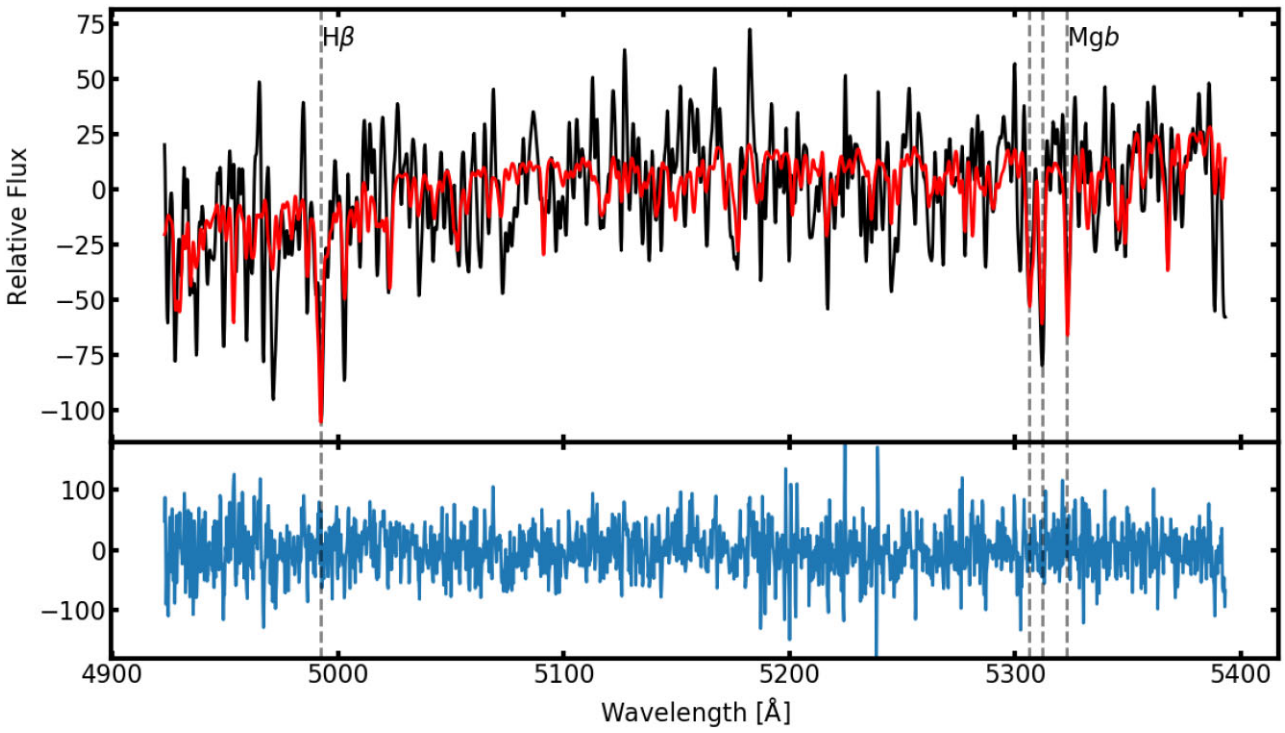

Figure 2. A Gaussian smoothed ($\sigma = 0.5$ Å) KCWI spectrum for Y358 (black) with example `pPXF` fit (red). Residuals from the non-smoothed fit are shown at the bottom (blue). The spectrum, fit, and residuals are displayed at the observed wavelengths. The prominent H β and Mg*b* triplet absorption features are indicated by dashed vertical lines.

$$M(< R_{1/2}) = 930 \left(\frac{\sigma_e^2}{\left(\mathrm{km\ s^{-1}}\right)^2} \right) \left(\frac{R_{\mathrm{e,circ}}}{\mathrm{pc}} \right) \mathrm{M_\odot}; \quad (1)$$

where $R_{1/2} \approx \frac{4}{3} R_{\mathrm{e,circ}}$

We note this equation requires the luminosity-weighted line-of-sight velocity dispersion within the half-light radius. Our extracted region on Y358 corresponds to a $\sim 6.3 \times 6.7$ arcsec^2 region, which is only slightly smaller than the effective diameter ($\sim$9 arcsec). Our measured velocity dispersion of 19 ± 3 km s^{-1} should well approximate the required value for equation (1). We therefore calculate a dynamical mass of $7.1 \pm 2.2 \times 10^8$ M$_\odot$ within 2.8 kpc for Y358 using equation (1).

3.1 Y358 halo mass

In Fig. 3, we compare the halo mass estimated from GC counts to the dynamical mass measurement we have obtained using our KCWI data. The comparison of a total halo mass to a mass measurement made within a fixed radius requires the assumption of a dark matter halo profile. Here, we assume a cuspy, NFW (Navarro, Frenk & White 1996) halo profile along with a cored, Di Cintio et al. (2014) halo profile. We additionally plot a halo of mass roughly expected for a GC-poor UDG ($N_{\mathrm{GC}} = 2$; $M_{\mathrm{Halo}} = 10^{10}$ M$_\odot$; Burkert & Forbes 2020) for each of the cuspy/cored profiles.

When the profile is forced to be a cuspy NFW profile with normal concentration (i.e. a concentration from Dutton & Macciò 2014), a halo of total mass $\sim 6.6 \times 10^9$ M$_\odot$ is required to have the same enclosed mass as our measurement for Y358. Y358 residing in such a low mass dark matter halo is highly unexpected as it is below the Burkert & Forbes (2020) prediction from its rich GC system (i.e. $1.4 \pm 0.25 \times 10^{11}$ M$_\odot$). There is evidence in the literature that UDGs should obey this relationship (e.g. Gannon et al. 2022) therefore we suggest that Y358 does not reside in a low-mass NFW halo. We instead conclude that Y358 likely resides in a cored and/or low concentration halo profile, as it must do in order to obey the Burkert & Forbes (2020) relation. Previous works studying UDG dynamical masses have come to similar conclusions for other UDGs (e.g. van Dokkum et al. 2019; Gannon et al. 2022).

3.2 Comparison to gas-rich UDGs

Recent work has suggested some isolated, gas-rich field UDGs may reside in low concentration and/or cored dark matter haloes (see e.g. Brook et al. 2021; Kong et al. 2022; Mancera Piña et al. 2022). Using resolved HI kinematics for seven such gas-rich isolated UDGs, Kong et al. (2022) were able to fit Read et al. (2016) mass profiles. Their best-fitting parameters are listed in their table 1. Read et al. (2016) mass profiles have the benefit of being able to reproduce observed dark matter cores in the dwarf halo mass regime while providing a convenient fitting function for star/gas kinematics.

We plot these best-fitting Read et al. (2016) mass profiles from Kong et al. (2022) for comparison to UDG stellar kinematics in Fig. 4 *upper*. We note that our GC-rich UDGs are primarily in the cluster environment and hence gas poor. The contribution of baryons to their calculated dynamical mass is therefore small ($\lessapprox$10 per cent) and they are extremely dark matter dominated in their dynamics. In contrast for the gas-rich UDGs, the gaseous component contributes significantly to the centrally enclosed mass (see e.g. the total masses in Kong et al. 2022, table 1). We therefore choose to compare our data to the Read et al. (2016) mass profiles for the gas-rich UDGs as these trace the dark matter component of the halo, which are more appropriate to compare to the measurements we are getting for our GC-rich/poor UDGs.

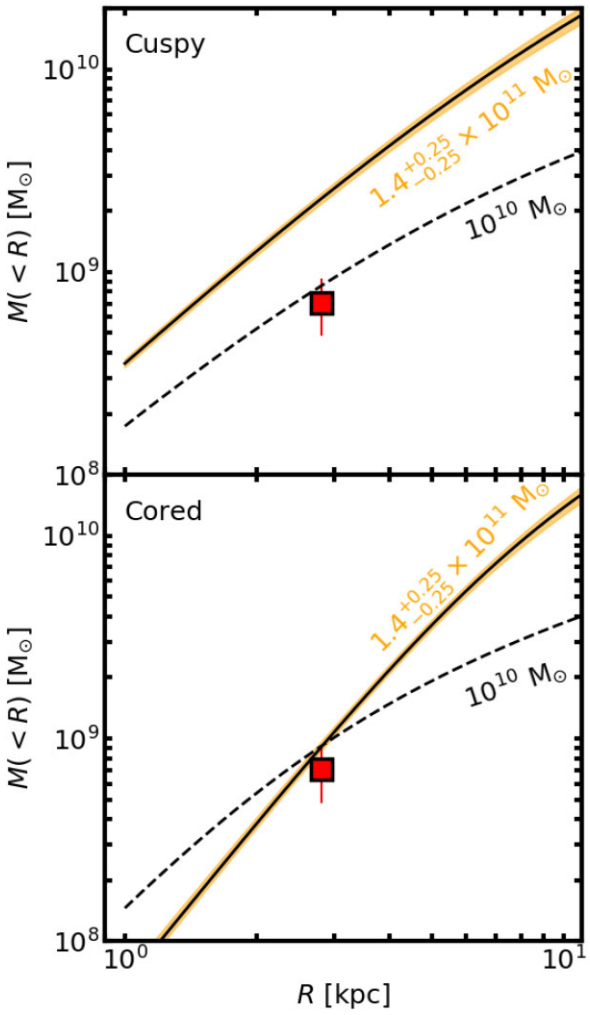

Figure 3. Enclosed mass versus galactocentric radius. We plot our dynamical mass measurement for Y358 (red square). In both panels, we plot a halo profile of total mass expected from Y358's GC richness and the relationship of Burkert & Forbes (2020; solid line with orange shading corresponding to the GC count uncertainty). We also include a halo profile of total mass roughly expected for a GC-poor UDG (i.e. $N_{\mathrm{GC}} = 2$, $M_{\mathrm{Halo}} = 10^{10}$ M$_\odot$; dashed line). In the upper panel, we plot these halo masses as cuspy NFW haloes, and in the lower panel, we plot them as cored Di Cintio et al. (2014) haloes. For Y358 to reside in a dark matter halo of mass expected from its GC counts, it likely resides in a cored dark matter halo.

In Fig. 4 *upper*, we plot our dynamical mass measurement for Y358 along with dynamical mass measurements for UDGs with stellar velocity dispersions and GC counts from Gannon et al. (2022). The UDGs in this sample are generally expected to be older and gas-poor due to their association with clusters. Only one of these UDGs is not associated with a cluster (i.e. NGC 5846_UDG1) and it is in a group environment. UDGs from the Gannon et al. (2022) sample have stellar masses in the range $8.04 < \log(M_\star / \mathrm{M_\odot}) < 8.89$. Four of the seven, Kong et al. (2022) UDGs have stellar masses in this range, with the remaining three having stellar masses slightly smaller (i.e. $7.45 < \log(M_\star / \mathrm{M_\odot}) < 8.35$). Plotted mass measurements are colour coded by GC-richness based on a rich/poor divide of $N_{\mathrm{GC}} \geq 20$ / $N_{\mathrm{GC}} < 20$. The halo mass implied for a GC-rich UDG with $N_{\mathrm{GC}} \geq 20$

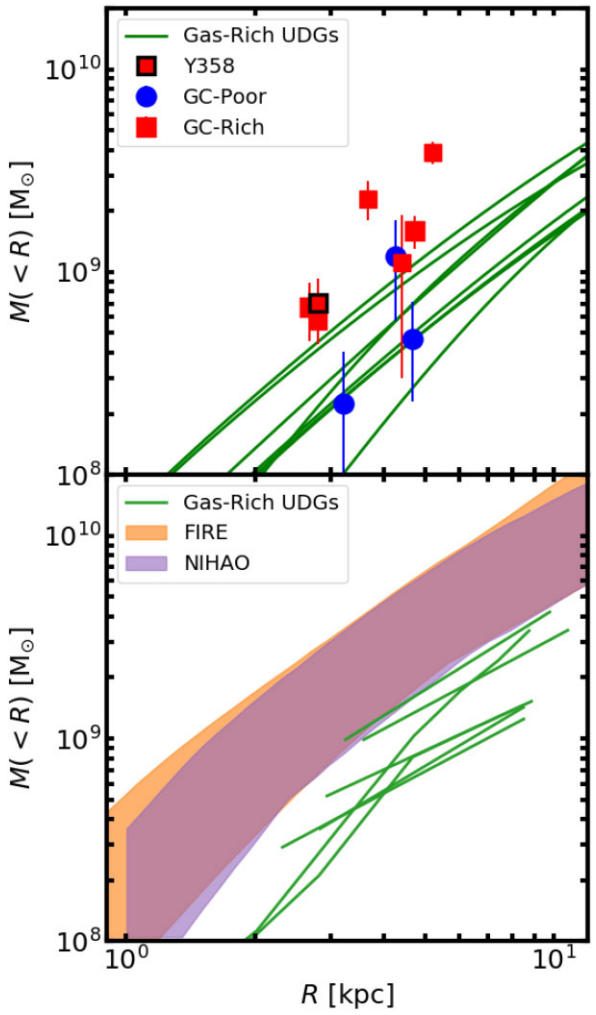

Figure 4. Enclosed mass versus galactocentric radius. *Upper:* Dynamical mass measurements for UDGs are plotted from Gannon et al. (2022; unbordered red and blue symbols) along with our Y358 dynamical mass measurement (black border). UDGs with rich ($N_{GC} > 20$) GC systems are plotted as red squares. UDGs with poor ($N_{GC} < 20$) GC systems are plotted as blue circles. The dark matter component of the best-fitting Read, Agertz & Collins (2016) halo profile to observations of gas-rich field UDGs are shown as green lines (see their equation 4 and table 1 Kong et al. 2022). For the Kong et al. (2022) UDGs, we exclude the gaseous component of their mass as our UDGs are dark matter dominated without gas. Dynamical mass measurements for GC-rich UDGs are on average too high for their formation to be easily explained as the transformation of the isolated, gas-rich Kong et al. (2022) UDGs. *Lower:* The observed HI mass profiles from Kong et al. (2022) now include the mass from stars and gas (green lines). We include the range of halo mass profiles reproduced by the NIHAO simulations of Di Cintio et al. (2017, purple shaded region) and the FIRE simulations of Chan et al. (2018, orange shaded region). For NIHAO, these profiles include the gas, stars, and dark matter. The FIRE-simulated mass profiles do not include gas as they artificially quench their galaxies as part of their simulation. Both the NIHAO simulations and the FIRE simulations predict mass profiles more massive than the observed UDGs of Kong et al. (2022). This is despite the observed UDGs and the simulated UDGs being in isolated environments.

is $\geq 10^{11}$ $M_\odot$ (Burkert & Forbes 2020). We summarize the pertinent properties (i.e. stellar mass, halo mass, environment, and gas content) of these two observational samples in Table 1.

It is clear from Fig. 4 *upper* that the GC-rich UDGs have dynamical masses that are too high to agree with the best-fitting dark matter haloes from Kong et al. (2022). We note that this may be a reflection of the different total halo masses of the two UDG populations. i.e. the best-fitting total halo masses of the isolated, gas-rich UDG in Kong et al. (2022) are all below $10^{10.8}$ $M_\odot$, which is less than the minimum inferred halo mass for a GC-rich UDG with $N_{GC}>20$ (10^{11} $M_\odot$; Burkert & Forbes 2020). Additionally, gas-rich UDGs tend to be younger, bluer with more irregular morphologies than other UDGs (Leisman et al. 2017), likely indicating ongoing star formation. Furthermore, recent work has shown that isolated, gas-rich UDGs do not have rich GC systems (Jones et al. 2022). We conclude that gas-rich UDGs similar to those observed by Kong et al. (2022) could not evolve into the GC-rich UDGs observed at present times. The progenitors of GC-rich UDGs require more massive dark matter haloes at fixed stellar mass.

This conclusion is not true for the GC-poor UDGs plotted in Fig. 4. All three of these UDGs have dynamical masses in agreement with the mass profiles of Kong et al. (2022). We suggest it is possible that GC-poor UDGs in clusters have similar dark matter halo characteristics to isolated, gas-rich UDGs. Further, this suggests the processing and passive evolution of isolated, gas-rich UDGs is a possible formation pathway for GC-poor UDGs in clusters. This conclusion is similar to proposals from previous works (see e.g. Román & Trujillo 2017b; Martin et al. 2019; Grishin et al. 2021). Our results therefore support GC-rich UDGs forming in more massive dark matter haloes than GC-poor UDGs, with GC-poor UDGs being the possible evolution of isolated, gas-rich UDGs.

In Fig. 4 *lower*, we plot the mass range of UDG profiles modelled in the NIHAO simulations of Di Cintio et al. (2017, purple band) and in the FIRE simulations of Chan et al. (2018, orange band) versus the observed isolated, gas-rich UDGs from Kong et al. (2022, green lines). Both simulations primarily model UDGs as 'puffy dwarfs' with large sizes driven by strong supernovae feedback. Both of the simulations are restricted to modelling UDGs in a relatively isolated environment, similar to the environment of Kong et al. (2022)'s observations. Additionally, the stellar mass range and total halo mass range of the UDGs modelled in the simulations provides good coverage of the stellar mass range and best-fitting total halo mass range of Kong et al. (2022)'s observed UDGs. We note, however, the recent observational work of Kado-Fong et al. (2022), which found that isolated, gas-rich UDGs do not exhibit the bursty star formation histories expected from these simulations. We summarize the stellar mass, total halo mass, environment, and gas-richness of each sample in Table 1. With similar environments, stellar masses, and total halo masses, we might expect these simulations to reproduce the mass profiles of the observed isolated, gas-rich UDGs.

To make this comparison, in Fig. 4 *lower*, we now plot the observed HI mass profiles from Kong et al. (2022), which include both the gaseous and stellar component of the mass along with the dark matter. The Di Cintio et al. (2017) NIHAO result plotted is also a total mass profile, including stars, gas, and dark matter. Note that the FIRE mass profiles do not include gas, as they artificially quench their UDGs as part of their simulation. Without this artificial quenching, their UDGs may still be expected to be gas-rich at present times. For both the Di Cintio et al. (2017) and Kong et al. (2022) data plotted in Fig. 4 *lower*, the gas mass is, on average, more massive than the stellar component.

It is clear from Fig. 4 *lower* that both simulations create mass profiles more massive than the isolated, gas-rich UDGs that their simulations are best matched to reproduce. This is despite having a similar total halo mass. The mass profiles from the simulations are instead more closely matched to the GC-rich UDGs plotted in the *upper* panel. However, few GC-rich UDGs have been observed in the

Table 1. Pertinent properties of UDG samples relating to the discussion of Fig. 4. From left-to-right columns are: (1) Sample description. When relevant, the simulation name is given before the literature reference; (2) Stellar mass range; (3) Halo mass range; (4) Environment; and (5) Gas content of the sample. The halo mass range of Cardona-Barrero et al. (2020) was not published in that work and was provided upon request by the corresponding author.

Sample	$\mathrm{Log}(M_\star/\mathrm{M}_\odot)$	$\mathrm{Log}(M_{\mathrm{Halo}}/\mathrm{M}_\odot)$	Environment	Gas content
Observed: Y358	8.14	11.06 − 11.22	Cluster	None
Observed: GC-Rich	8.04 − 8.89	>11	Cluster/Group	None
Observed: GC-Poor	8.41 − 8.76	<11	Cluster	None
Observed: Kong + (2022)	7.45 − 8.35	9.86 − 10.76	Field	Rich
NIHAO: Di Cintio + (2017)	6.83 − 8.4	10.22 − 10.85	Field	Rich
NIHAO: Jiang + (2018)	6.8 − 8.8	9.9 − 11.1	Field/Group	Rich
NIHAO: Cardona-Barrero + (2020)	6.5 − 9.0	10.04 − 11.29	Field	Rich
FIRE: Chan + (2018)	7.72 − 8.44	10.34 − 10.74	Field	None

low-density environments such as those simulated, with some authors suggesting environment plays a key role in their GC formation (Prole et al. 2019a; Somalwar et al. 2020). Furthermore, based on their GC-richness and the GC number – halo–mass relationship of Burkert & Forbes (2020), the GC-rich UDGs plotted are all expected to reside in haloes of total mass greater than either the FIRE or NIHAO simulations at the same stellar mass. In order to have the observed GC-rich UDGs residing in haloes with the total mass that is modelled in the simulations at the same stellar mass, they cannot follow the Burkert & Forbes (2020) relationship. We explore UDGs in stellar mass–halo mass space further in Section 3.3.

It is worth noting that further studies of UDGs in the NIHAO simulations have shown that NIHAO can model UDGs in group environments and at higher stellar masses (Jiang et al. 2019; Cardona-Barrero et al. 2020). It is therefore likely that the full mass profile range that is reproducible by the NIHAO simulations is not fully captured by what we are plotting from Di Cintio et al. (2017). However, UDGs at higher stellar masses are expected to have higher mass profiles (see Table 1). These higher stellar mass UDGs will therefore not affect the conclusions we draw from Fig. 4 *lower*. Additionally, some of the UDG sample used in Di Cintio et al. (2017) includes galaxies that do not strictly meet the original van Dokkum et al. (2015) UDG definition (i.e. they include galaxies with $R_e < 1.5$ kpc).

3.3 UDGs on the stellar mass–halo mass relationship

In Fig. 5, we further investigate observed UDGs versus the FIRE and NIHAO simulations by comparing them with the stellar mass–halo mass relationship. Y358 and GC-rich UDGs from Gannon et al. (2022) are plotted using halo mass measurements calculated from their GC-numbers (Burkert & Forbes 2020). Here, we do not plot the UDGs PUDG_S74 and PUDG_R84, along with the GC-poor sample,

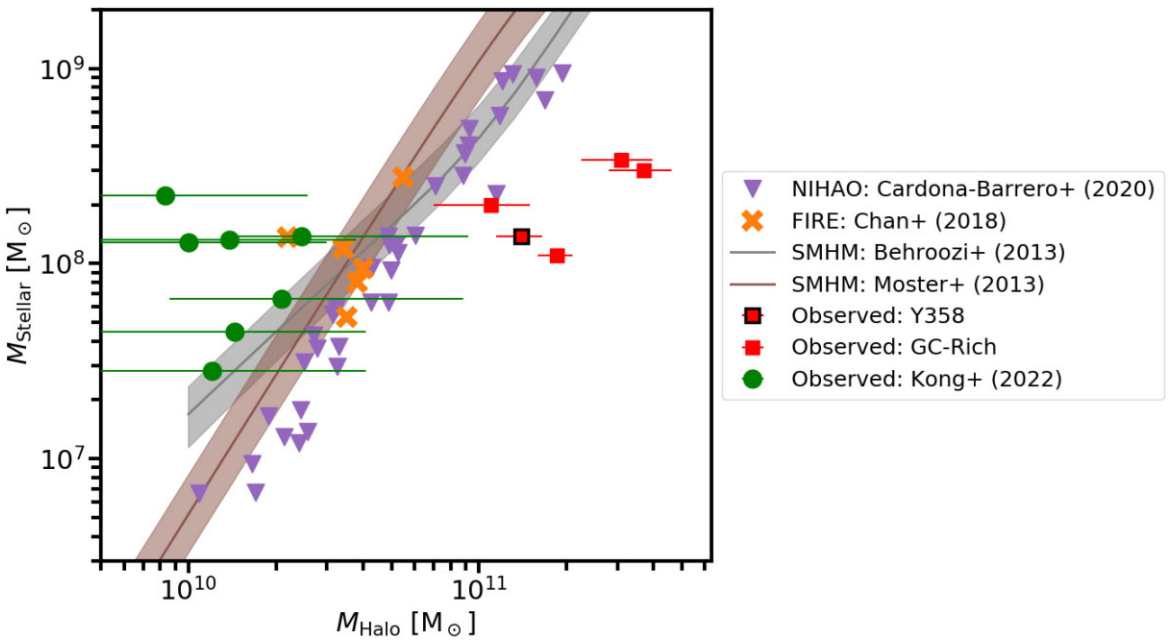

Figure 5. Stellar mass versus halo mass. We plot Y358 (black border) along with other GC-rich UDGs from Gannon et al. (2022) as red squares. The isolated, gas-rich UDGs of Kong et al. (2022) UDGs are shown as green circles. The simulated FIRE UDGs are shown as orange crosses with NIHAO UDGs from Cardona-Barrero et al. (2020) as purple triangles. Stellar mass–halo mass relations are shown from Behroozi, Wechsler & Conroy (2013, grey line and shaded band) and Moster, Naab & White (2013, brown line and shaded band). Both simulations create UDGs that generally follow conventional stellar mass–halo mass relations. The observed GC-rich UDGs have halo masses more massive than either stellar mass–halo mass relationship at fixed stellar masses. The observed isolated, gas-rich UDGs from Kong et al. (2022) have halo masses less massive than either stellar mass–halo mass relationship at fixed stellar masses. Neither observed sample is reproduced by the FIRE or NIHAO simulations.

Table 2. A summary of the deviations from the stellar mass–halo mass relationships of Behroozi et al. (2013) and Moster et al. (2013) for each sample using equation (2). From left-to-right columns are: (1) the sample; (2) the number of objects in the sample; (3) Δ_{B13}, the average deviation calculated for Behroozi et al. (2013); and (4) Δ_{M13}, the average deviation calculated for Moster et al. (2013). Note that Y358 is included in the calculation of the GC-rich statistics.

Sample	n	Δ_{B13} (dex)	Δ_{M13} (dex)
Observed: Y358	1	0.49	0.54
Observed: GC-Rich	5	0.53	0.63
Observed: Kong + (2022)	7	− 0.37	− 0.38
NIHAO: Cardona-Barrero + (2020)	37	0.11	0.16
FIRE: Chan + (2018)	6	− 0.03	− 0.01

as their exact GC counts with errors are unpublished, leading to an uncertain total halo mass. Kong et al. (2022) UDGs are plotted using the total halo mass coming from best-fitting Read et al. (2016) halo profiles (see their table 1). The data for the NIHAO sample presented in Cardona-Barrero et al. (2020) were attained from the corresponding author. The data for the FIRE UDGs are taken from their table 2 (Chan et al. 2018). Stellar mass–halo mass relationships are plotted from the studies of Behroozi et al. (2013) and Moster et al. (2013).

To quantify the deviation of each sample plotted in Fig. 5 from established stellar mass–halo mass relationships, we define the quantity Δ_{SMHM} for a sample of size n. This is the average logarithmic difference between the measured halo masses $M_{halo,\,UDG}$ and the expected halo mass at the stellar mass of each UDG $M_{halo,\,SMHM}$ based on a stellar mass–halo mass relationship.

$$\Delta_{SMHM} = \frac{1}{n}\sum_{i=1}^{n} \log_{10}\frac{M_{Halo,UDG}}{M_{Halo,SMHM}} \quad (2)$$

When using equation (2) for Behroozi et al. (2013) and Moster et al. (2013), we refer to it as Δ_{B13} and Δ_{M13}, respectively. Positive values for Δ_{SMHM} indicate that the sample resides in dark matter haloes that are, on average, more massive than the stellar mass–halo mass relationship. Negative values for Δ_{SMHM} indicate that the sample resides in dark matter haloes that are, on average, less massive than the stellar mass–halo mass relationship. Values of Δ_{SMHM} near zero indicate the sample obeys the relationship. We summarize the values of Δ_{SMHM} in Table 2. Note that seven of the Cardona-Barrero et al. (2020) UDGs are excluded from the calculation of Δ_{B13} as they have stellar masses below the relationship's minimum value ($M_{\star,\,Min} = 1.7 \times 10^7$ M$_\odot$).

It is clear from Fig. 5 and Table 2 that both simulated UDG samples largely follow known stellar mass–halo mass relations (average $|\Delta_{SMHM}| < 0.2$ dex). This is less than the typical scatter (0.2 dex) in these relations. The only exception is the low-mass (both stellar and total halo) end of the Cardona-Barrero et al. (2020) data, which does not follow Behroozi et al. (2013). In contrast, both observational samples deviate strongly from both stellar mass–halo mass relations. The isolated, gas-rich UDGs of Kong et al. (2022) reside in haloes less massive than the stellar mass–halo mass relation predicts for their stellar mass ($\Delta_{B13} = -0.37$ dex; $\Delta_{M13} = -0.38$ dex). This conclusion has been reached previously for a similar UDG sample by Trujillo-Gomez, Kruijssen & Reina-Campos (2022). Note also that, it is unlikely that the low halo masses of these UDGs are caused by tidal stripping due to their isolated environments. The GC-rich UDG sample (which includes Y358) resides in haloes more massive than the stellar mass–halo mass relationship predicts for their stellar mass ($\Delta_{B13} = 0.53$ dex; $\Delta_{M13} = 0.63$ dex). Despite both FIRE and NIHAO reproducing the observed dynamical masses of GC-rich UDGs (Fig. 4), they do not reproduce their inferred halo mass at their stellar mass.

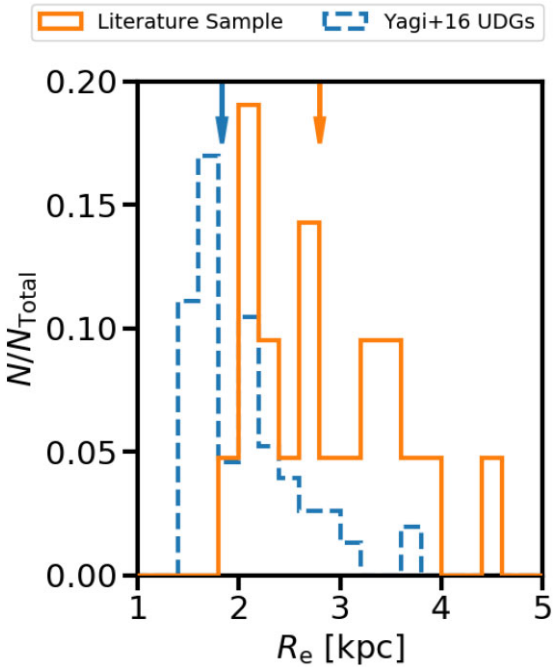

Figure 6. Normalized histograms of UDG circularized half-light radii. We plot our UDG sample ($N = 21$; orange solid line) in comparison to the Yagi et al. (2016) R-band catalogue of Coma cluster objects that are UDGs ($N = 153$; blue dashed line). Median values for each sample are indicated by arrows at the top of the plot. Our UDG sample has generally larger half-light radii than the Coma sample.

4 EXTENDED LITERATURE SAMPLE

For the remainder of this paper, we supplement our data for Y358 with data taken from the literature for spectroscopically studied UDGs. We take those galaxies from the literature that meet a UDG definition of $R_e > 1.5$ kpc and $\langle\mu_V\rangle_e > 24.7$ mag arcsec^{-2}. Our surface brightness criterion is simply that is used in Gannon et al. (2022), $\langle\mu_g\rangle_e > 25$ mag arcsec^{-2}, transformed into V-band with a colour of $V = g - 0.3$. We have identified 21 galaxies in the literature meeting this definition with basic properties to place them in mass–radius–luminosity space. These properties (i.e. identifier, environment, distance, Mag., $\langle\mu_V\rangle_e$, stellar mass, R_e, recessional velocity, velocity dispersion, and GC counts) are listed in Table A1. We include notes as to the construction of this sample in Appendix A.

4.1 UDG spectroscopic sample biases

We note our UDG sample originates from a wide range of literature sources and therefore is not complete. We therefore briefly mention two obvious biases in the sample. Namely, UDGs in our literature sample tend to be (1) larger and (2) brighter in surface brightness than the broader UDG population.

In Fig. 6, we plot a histogram of UDG sizes for both our literature UDG sample and a subset of the R-band Coma cluster catalogue of Yagi et al. (2016) that are UDGs ($R_e > 1.5$ kpc and $\langle\mu_R\rangle_e > 25$ mag arcsec^{-2}). We use this sample due to their likely association with the Coma Cluster, which will decrease the uncertainty in their

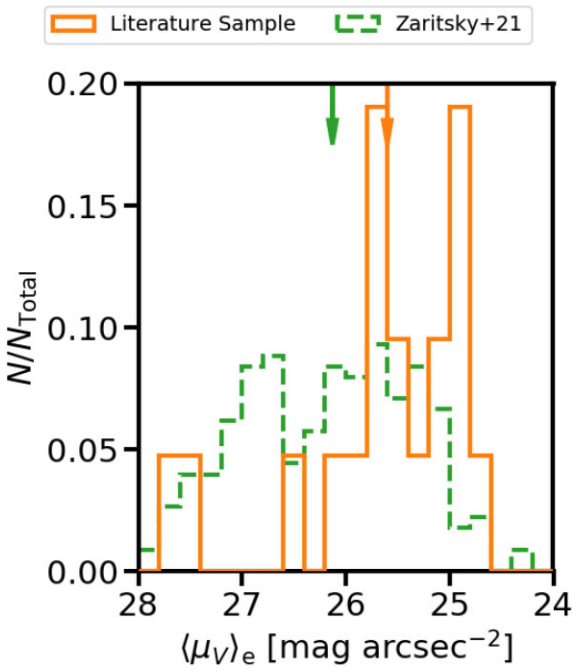

Figure 7. Normalized histograms of UDG surface brightnesses. We plot our UDG sample ($N = 21$; orange solid line) in comparison to UDG candidates in the Stripe82 region ($N = 226$; green dashed line; Zaritsky et al. 2021). Median values for each sample are indicated by arrows at the top of the plot. Our UDG sample has brighter surface brightnesses on average than UDGs in the Stripe82 region.

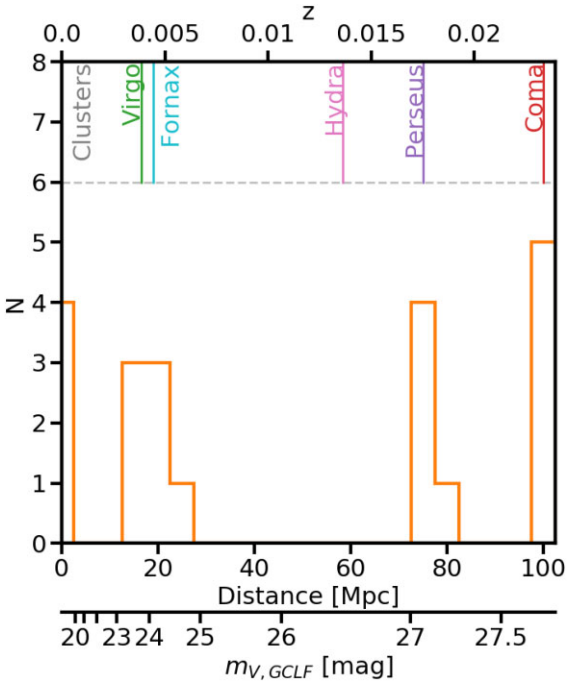

Figure 8. A histogram of UDG distances for UDGs from our literature sample. The *x*-axis shows the distance (Mpc), redshift (z), and the apparent magnitude of the GC luminosity function peak. The positions of select clusters are given along the top of the plot (vertical coloured lines). To date, no UDGs have been targeted for deep spectroscopy at distances beyond 100 Mpc.

true size in comparison to a UDG sample of unknown distance. The use of a catalogue in a different filter band is expected to have only a small ($\approx$ 10 per cent) effect on half-light radii (see e.g. the UDG fitting in table 2 of Saifollahi et al. 2022), which is not large enough to affect our results. Performing a Kolmogorov–Smirnov test, it is highly unlikely that our UDG sample was randomly selected from the UDGs in the Yagi et al. (2016) catalogue (p value = 0.005). Our literature sample is larger, with median half-light radius (2.8 kpc) larger than the Yagi et al. (2016) catalogue (median half-light radius 1.83 kpc).

In Fig. 7, we plot a histogram of the surface brightnesses of our literature UDG sample. We include for comparison UDG candidates from the Stripe 82 SMUDGes catalogue of Zaritsky et al. (2021). Here, we do not reuse the Yagi et al. (2016) catalogue due to the need for a common filter band to compare surface brightnesses. Additionally, the Zaritsky et al. (2021) catalogue provides the benefit of having UDGs across a full range of environments (field to cluster). For the Zaritsky et al. (2021) data, we convert their measured central surface brightnesses to the average within the half-light radius using equation 11 of Graham & Driver (2005) for comparison to our other data. We also correct this g-band catalogue into V-band using $V = g - 0.3$. Performing a Kolmogorov–Smirnov test, it is unlikely that our UDG sample was randomly selected from the Zaritsky et al. (2021) catalogue (p value = 0.012). Our literature sample has a median surface brightness (25.6 mag arcsec^{-2}) brighter than the Zaritsky et al. (2021) catalogue (median surface brightness 26.1 mag arcsec^{-2}). We note that this is despite the Zaritsky et al. (2021) catalogue containing blue UDGs, which will create a bias in their sample to be brighter due to their younger ages.

To further contextualize our literature sample, we show a histogram of their distances in Fig. 8. We include the peak of the GC luminosity function at each distance based on an assumed peak of $M_V = -7.3$ (Miller & Lotz 2007). We also include a number of commonly studied clusters. To date, no UDGs have been targeted for deep spectroscopy at distances beyond 100 Mpc.

In order to best establish dark matter halo profile parameters, accurate radial mass profiles are required. For UDGs, a thorough exploration of their likely cored dark matter haloes will require observations to be made beyond the dark matter core radius (~5–10 kpc). The current single mass measurements available for many UDGs are insufficient to truly establish dark matter halo parameters due to degeneracies in their comparison to theoretical halo mass profiles (Gannon et al. 2021). GCs pose a promising avenue to get larger radius mass estimates for UDGs to help probe their halo profile (e.g. Gannon et al. 2020). Importantly, this suggests UDG observational efforts should be focused on those candidates nearby enough to allow spectroscopic studies of their GC system.

5 DISCUSSION: MASS–RADIUS–LUMINOSITY SPACE

In Fig. 9, we place UDGs in mass–radius–luminosity space, an altered form of the fundamental plane for pressure-supported systems. We establish the locus traced by non-UDGs using data from Tollerud et al. (2011), Toloba et al. (2012), McConnachie (2012), Kourkchi et al. (2012), and Forbes et al. (2018). For Toloba et al. (2012) galaxies, we convert half-light radii into physical units using an assumed Virgo cluster distance of 16.5 Mpc. We place Kourkchi et al. (2012) galaxies on the plane using a correction of $V = F814W + 1$. We place McConnachie (2012)[1] galaxies on the plane using their

[1]January 2021 public version

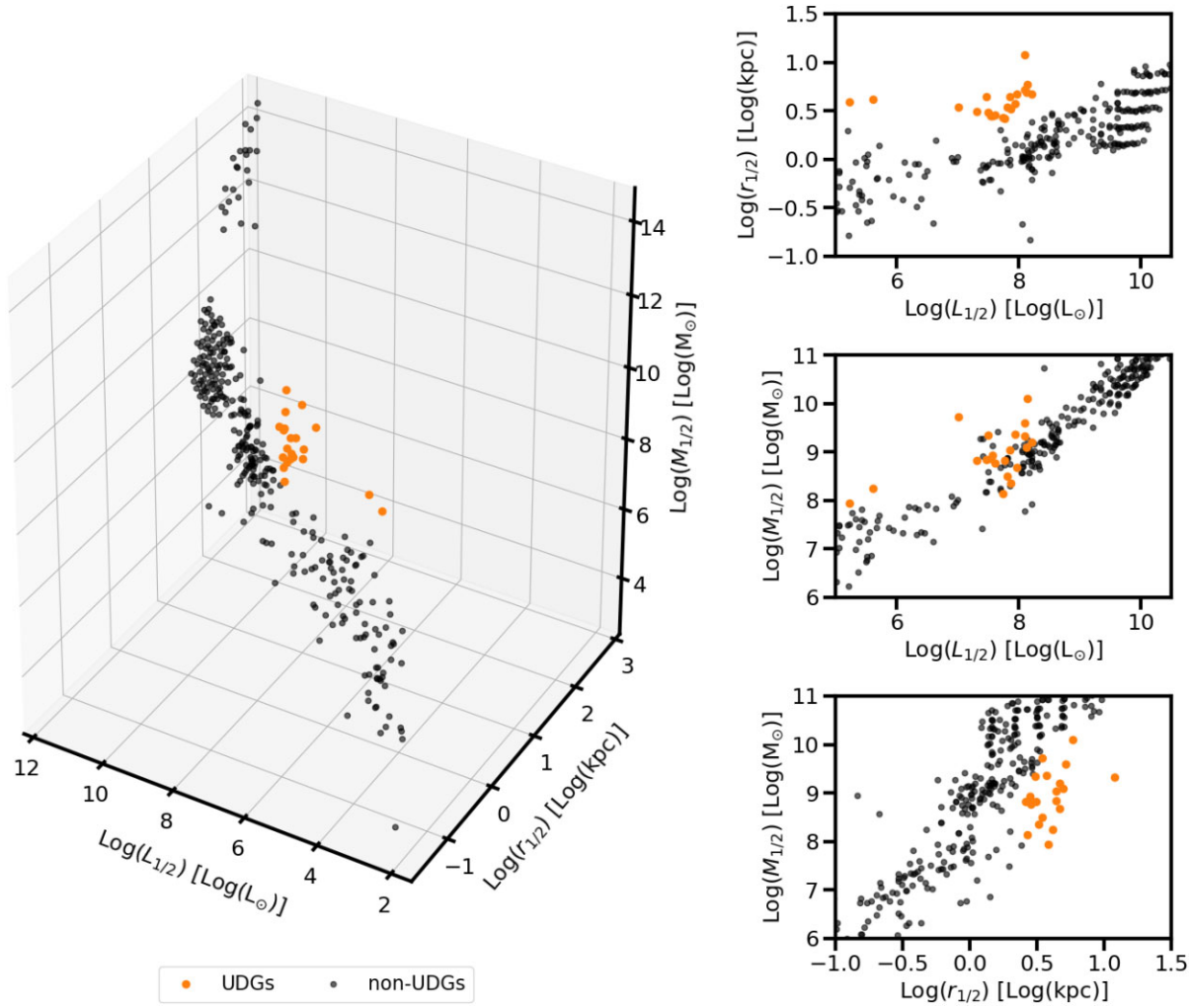

Figure 9. *Left:* Mass–radius–luminosity space: half-light luminosity ($L_{1/2}$), half-light radius ($r_{1/2}$) and dynamical mass within the half-light radius ($M_{1/2}$). We project the plane and zoom around the location of UDGs on the *Right*. From top to bottom, these are the $L_{1/2} - r_{1/2}$, $L_{1/2} - M_{1/2}$, and $r_{1/2} - M_{1/2}$ projections of the plane. We establish the locus for non-UDGs using the data from Tollerud et al. (2011), Toloba et al. (2012), McConnachie (2012), Kourkchi et al. (2012), and Forbes et al. (2018; black points). See text for more details on these data. We also include our UDG sample on the plane (orange). UDGs are located off the locus for normal galaxies with the primary difference being their larger sizes.

given Vega magnitudes. We then place our literature UDG sample on the plane to examine their location. We convert magnitudes into solar units assuming $M_{V,\,\mathrm{Sun}} = 4.8$ (Willmer 2018a) and dynamical masses are calculated using equation (1). Galaxies that fit the UDG definition in the non-UDG samples (e.g. the Sagittarius dSph appears in both McConnachie 2012 and Forbes et al. 2018) are removed before plotting as they are included in our literature sample.

We note two UDGs plotted, Andromeda XIX and Antlia II, have half-light luminosities noticeably less bright than the remaining population. These galaxies have measured velocity dispersions only due to their extremely close distances (i.e. both are in the Local Group), which allows their stars to be resolved. We note that there exists a continuum of galaxies of large size and varying luminosity between these galaxies and the remaining UDGs on the relation (see e.g. table 2 of Karachentsev et al. 2017). The empty region between these galaxies and the remainder of our sample is simply a side effect of our bias to higher surface brightness objects. For the remainder of our discussion, we will focus on the higher-luminosity objects more readily studied.

Interestingly, UDGs reside in a region of parameter space largely separate from the locus of non-UDGs. Their main difference is simply their larger half-light radii, with dynamical masses and luminosities similar to the locus of non-UDGs (the empty region between these two populations in half-light radii on Fig. 9 exists due to selection effects). An unfortunate corollary of UDGs inhabiting an entirely new parameter space is that, at fixed luminosity, UDG masses cannot be estimated from luminosity and radius information alone. This will hamper efforts to perform statistical estimations of UDG masses based on their photometric properties (e.g. Zaritsky 2017; Lee et al. 2020).

The similarity in luminosities between UDGs and non-UDGs have led many to suggest they may simply be an extension of the dwarf galaxy population to larger sizes (see e.g. Conselice 2018). These UDGs could be 'puffy' dwarf galaxies formed through conventional pathways (e.g. Amorisco & Loeb 2016; Di Cintio et al. 2017; Rong et al. 2017; Tremmel et al. 2020). A likely example of these are the GC-poor, cluster UDGs plotted in Fig. 4 that are plausibly the result of the transformation of extended, star-forming field dwarfs (e.g. Grishin et al. 2021). In mass–radius–luminosity space, 'puffy dwarf'

UDGs are expected to have similar luminosities, larger radii and dynamical masses only slightly larger than their non-UDGs of similar luminosity. This is reflective of their similar dark matter haloes. Much of our literature sample has mass, radius, and luminosity compatible with this expectation for a 'puffy dwarf' formation scenario.

We caution that this expectation for 'puffy dwarf' UDGs may be over-simplified. Kadowaki et al. (2021) found that the dynamical masses of UDGs measured with increasingly large radii likely correspond to increasingly massive dark matter haloes (see their appendix A). In this framework, many of the UDGs in our sample may have dynamical masses corresponding to dark matter haloes more massive than non-UDGs at similar luminosity. If this is the case, these UDGs cannot be explained by 'puffy dwarf' formation scenarios due to their massive dark matter haloes. We do note, however, that due to the bias to UDGs with larger half-light radius in our sample, we expect a greater fraction of our sample to be massive halo UDGs than the UDG population as a whole.

Finally, we suggest that Fig. 9 is a fundamental empirical plot that should be reproduced by galaxy formation simulations focusing on UDGs. Particularly, many simulations currently have difficulty reproducing the full range of dwarf galaxy sizes. For example, the ROMULUS-C simulations currently form the majority of their dwarfs in the UDG stellar mass regime as UDGs (see Tremmel et al. 2020, table 1). In addition, UDG studies using the Illustris simulations have to assign their UDG candidates sizes due to limitations of their simulations (Carleton et al. 2019; Sales et al. 2020). Simulations reproducing the full range of galaxy sizes and masses in the UDG luminosity regime will be crucial to developing a theoretical understanding of their formation.

6 CONCLUSIONS

In this work, we have added Keck/KCWI spectroscopy of a GC-rich, Coma cluster UDG, Y358, to the literature. We then create a literature sample of UDGs that have been studied spectroscopically, placing them in mass–radius–luminosity space for pressure-supported galaxies. Our main conclusions are as follows:

(i) We measure a recessional velocity (7969 $\pm$ 2 km s^{-1}) and velocity dispersion (19 $\pm$ 3 km s^{-1}) for Y358. The recessional velocity confirms its association with the Coma cluster. This association formalizes the distance of Y358 and its status as a UDG.

(ii) We calculate a dynamical mass for Y358 and compare it to cuspy and cored dark matter halo profiles with total mass inferred from its GC count. Under the assumption that the total halo mass from GC counts is correct, Y358 likely resides in a cored dark matter halo.

We supplement our dynamical mass measurement for Y358 with others from Gannon et al. (2022). We then compare to the best-fitting dark matter mass profiles for isolated, gas-rich UDGs from Kong et al. (2022). We also compare the Kong et al. (2022) measurements to simulations of UDG formation from the NIHAO suite (Di Cintio et al. 2017) and the FIRE suite (Chan et al. 2018). We find:

(iii) The GC-poor UDGs may reside in a dark matter halo of similar radial profile to the isolated, gas-rich UDGs of Kong et al. (2022), suggesting an evolutionary connection may exist between the two populations. Dynamical mass measurements made for GC-rich UDGs are sufficiently high to exclude them residing in dark matter haloes similar to the isolated, gas-rich UDGs. We suggest it is unlikely that GC-rich UDGs represent an evolved population of isolated, gas-rich UDGs.

(iv) Both the simulations of Di Cintio et al. (2017) and Chan et al. (2018) produce mass profiles for UDGs that are too massive when compared to the isolated, gas-rich UDGs of Kong et al. (2022). This is unexpected as the Kong et al. (2022) samples have the properties (i.e. stellar mass, total halo mass, environment, and gas-richness) most resembling the UDG in their simulations. The simulated mass profiles are instead more consistent with GC-rich UDGs.

(v) We find that although FIRE and NIHAO simulations cover the stellar and halo mass range of GC-rich UDGs, they cannot reproduce their observationally estimated halo masses at the same stellar mass. This is perhaps not unexpected given that the simulations are for isolated UDGs, whereas our observed UDGs are located in groups and clusters where additional environmental effects may play a role in their evolution.

We then gather a literature sample for all galaxies meeting our UDG definition with spectroscopic velocity dispersions. We find two biases in this sample:

(a) The UDGs in our literature sample are on average larger than the population as a whole.
(b) The UDGs in our literature sample have brighter surface brightness than the population as a whole.

Both of these need to be kept in mind when considering UDG formation scenarios from current observational data. We then place our UDG sample in mass–radius–luminosity space, examining their location. We find:

(vi) UDGs are located at a similar locus to non-UDGs of similar luminosity with the primary difference being their increased half-light radius. This supports notions that some UDGs are simply 'puffy dwarfs' with extended sizes driven by known physical processes.

(vii) UDGs' dynamical masses within their large radii may indicate massive dark matter haloes not expected in a 'puffy dwarf' formation scenario. As our UDG sample is biased to the largest systems, we suggest a greater fraction of UDGs in our sample may be massive halo UDGs than the population as a whole.

ACKNOWLEDGEMENTS

We thank the anonymous referee for their considered reading of this work and comments which have improved its quality. We thank S. Cardona-Barrero for providing us with their NIHAO data. We thank A. Alabi for aiding with the KCWI observations. JSG thanks R. Abraham, M. L. Buzzo, and S. Janssens for insightful conversations throughout the creation of this work. Some of the data presented herein were obtained at the W. M. Keck Observatory, which is operated as a scientific partnership among the California Institute of Technology, the University of California and the National Aeronautics and Space Administration. The Observatory was made possible by the generous financial support of the W. M. Keck Foundation. The authors wish to recognize and acknowledge the very significant cultural role and reverence that the summit of Maunakea has always had within the indigenous Hawaiian community. We are most fortunate to have the opportunity to conduct observations from this mountain. AJR was supported as a Research Corporation for Science Advancement Cottrell Scholar. JSG acknowledges financial support received through a Swinburne University Postgraduate Research Award throughout the creation of this work. AFM acknowledges support from the Severo Ochoa Excellence scheme (CEX2019-000920-S) and from grant PID2019-107427GB-C32 from the MCIU of Spain.

DATA AVAILABILITY

The KCWI data presented are available via the Keck Observatory Archive (KOA): https://www2.keck.hawaii.edu/koa/public/koa.php 18 months after observations are taken. The literature sample discussed is included in Appendix A.

REFERENCES

Alabi A. et al., 2018, MNRAS, 479, 3308
Amorisco N. C., Loeb A., 2016, MNRAS, 459, L51
Amorisco N. C., Monachesi A., Agnello A., White S. D. M., 2018, MNRAS, 475, 4235
Barbosa C. E. et al., 2020, ApJS, 247, 46
Beasley M. A., Romanowsky A. J., Pota V., Navarro I. M., Martinez Delgado D., Neyer F., Deich A. L., 2016, ApJ, 819, L20
Behroozi P. S., Wechsler R. H., Conroy C., 2013, ApJ, 770, 57
Borriello A., Salucci P., Danese L., 2003, MNRAS, 341, 1109
Bothun G. D., Impey C. D., Malin D. F., Mould J. R., 1987, AJ, 94, 23
Brook C. B., Di Cintio A., Macciò A. V., Blank M., 2021, ApJ, 919, L1
Burkert A., Forbes D. A., 2020, AJ, 159, 56
Buzzo M. L. et al., 2022, MNRAS, 517, 2231
Cappellari M. et al., 2006, MNRAS, 366, 1126
Cappellari M., 2017, MNRAS, 466, 798
Cardona-Barrero S., Di Cintio A., Brook C. B. A., Ruiz-Lara T., Beasley M. A., Falcón-Barroso J., Macciò A. V., 2020, MNRAS, 497, 4282
Carleton T., Errani R., Cooper M., Kaplinghat M., Peñarrubia J., Guo Y., 2019, MNRAS, 485, 382
Carleton T., Guo Y., Munshi F., Tremmel M., Wright A., 2021, MNRAS, 502, 398
Chan T. K., Kereš D., Wetzel A., Hopkins P. F., Faucher-Giguère C. A., El-Badry K., Garrison-Kimmel S., Boylan-Kolchin M., 2018, MNRAS, 478, 906
Chilingarian I. V., Afanasiev A. V., Grishin K. A., Fabricant D., Moran S., 2019, ApJ, 884, 79
Coelho P. R. T., 2014, MNRAS, 440, 1027
Cohen Y. et al., 2018, ApJ, 868, 96
Collins M. L. M., Tollerud E. J., Rich R. M., Ibata R. A., Martin N. F., Chapman S. C., Gilbert K. M., Preston J., 2020, MNRAS, 491, 3496
Conselice C. J., 2018, Res. Notes Am. Astron. Soc., 2, 43
Dalcanton J. J., Spergel D. N., Gunn J. E., Schmidt M., Schneider D. P., 1997, AJ, 114, 635
Danieli S. et al., 2022, ApJ, 927, L28
Danieli S., van Dokkum P., Conroy C., Abraham R., Romanowsky A. J., 2019, ApJ, 874, L12
Di Cintio A., Brook C. B., Dutton A. A., Macciò A. V., Obreja A., Dekel A., 2017, MNRAS, 466, L1
Di Cintio A., Brook C. B., Dutton A. A., Macciò A. V., Stinson G. S., Knebe A., 2014, MNRAS, 441, 2986
Disney M. J., 1976, Nature, 263, 573
Djorgovski S., Davis M., 1987, ApJ, 313, 59
Dressler A., 1987, ApJ, 317, 1
Dutton A. A., Macciò A. V., 2014, MNRAS, 441, 3359
Emsellem E. et al., 2019, A&A, 625, A76
Faber S. M., Dressler A., Davies R. L., Burstein D., Lynden Bell D., Terlevich R., Wegner G., 1987, in Faber S. M., ed., Nearly Normal Galaxies. From the Planck Time to the Present. p. 175
Ferré-Mateu A. et al., 2018, MNRAS, 479, 4891
Forbes D. A., Alabi A., Romanowsky A. J., Brodie J. P., Arimoto N., 2020a, MNRAS, 492, 4874
Forbes D. A., Dullo B. T., Gannon J., Couch W. J., Iodice E., Spavone M., Cantiello M., Schipani P., 2020b, MNRAS, 494, 5293
Forbes D. A., Gannon J. S., Romanowsky A. J., Alabi A., Brodie J. P., Couch W. J., Ferré-Mateu A., 2021, MNRAS, 500, 1279
Forbes D. A., Gannon J., Couch W. J., Iodice E., Spavone M., Cantiello M., Napolitano N., Schipani P., 2019, A&A, 626, A66
Forbes D. A., Lasky P., Graham A. W., Spitler L., 2008, MNRAS, 389, 1924
Forbes D. A., Read J. I., Gieles M., Collins M. L. M., 2018, MNRAS, 481, 5592
Gannon J. S. et al., 2021, MNRAS, 502, 3144
Gannon J. S. et al., 2022, MNRAS, 510, 946
Gannon J. S., Forbes D. A., Romanowsky A. J., Ferré-Mateu A., Couch W. J., Brodie J. P., 2020, MNRAS, 495, 2582
Graham A. W., Driver S. P., 2005, Publ. Astron. Soc. Aust., 22, 118
Graves G. J., Faber S. M., 2010, ApJ, 717, 803
Grishin K. A., Chilingarian I. V., Afanasiev A. V., Fabricant D., Katkov I. Y., Moran S., Yagi M., 2021, Nature Astron., 5, 1308
Habas R. et al., 2020, MNRAS, 491, 1901
Harris W. E., Blakeslee J. P., Harris G. L. H., 2017, ApJ, 836, 67
Ibata R., Irwin M., Lewis G. F., Stolte A., 2001, ApJ, 547, L133
Impey C., Bothun G., 1997, ARA&A, 35, 267
Impey C., Bothun G., Malin D., 1988, ApJ, 330, 634
Janssens S. R. et al., 2022, MNRAS, 517, 858
Janssens S. R., Abraham R., Brodie J., Forbes D. A., Romanowsky A. J., 2019, ApJ, 887, 92
Janssens S., Abraham R., Brodie J., Forbes D., Romanowsky A. J., van Dokkum P., 2017, ApJ, 839, L17
Jiang F., Dekel A., Freundlich J., Romanowsky A. J., Dutton A. A., Macciò A. V., Di Cintio A., 2019, MNRAS, 487, 5272
Jones M. G. et al., 2022, preprint (arXiv:2211.00651)
Kado-Fong E., Greene J. E., Huang S., Goulding A., 2022, ApJ, preprint (arXiv:2209.05492)
Kadowaki J., Zaritsky D., Donnerstein R. L. R. S. P., Karunakaran A., Spekkens K., 2021, ApJ, 923, 257
Karachentsev I. D., Karachentseva V. E., Suchkov A. A., Grebel E. K., 2000, A&AS, 145, 415
Karachentsev I. D., Makarova L. N., Sharina M. E., Karachentseva V. E., 2017, Astrophys. Bull., 72, 376
Keim M. A. et al., 2022, ApJ, 935, 160
Kong D., Kaplinghat M., Yu H.-B., Fraternali F., Mancera Piña P. E., 2022, ApJ, 936, 166
Kourkchi E. et al., 2012, MNRAS, 420, 2819
La Marca A. et al., 2022, A&A, 665, A105
Leaman R., Cole A. A., Venn K. A., Tolstoy E., Irwin M. J., Szeifert T., Skillman E. D., McConnachie A. W., 2009, ApJ, 699, 1
Lee J. H., Kang J., Lee M. G., Jang I. S., 2020, ApJ, 894, 75
Leisman L. et al., 2017, ApJ, 842, 133
Lewis G. F., Brewer B. J., Wan Z., 2020, MNRAS, 491, L1
Liao S. et al., 2019, MNRAS, 490, 5182
Lim S. et al., 2020, ApJ, 899, 69
Lim S., Peng E. W., Côté P., Sales L. V., den Brok M., Blakeslee J. P., Guhathakurta P., 2018, ApJ, 862, 82
Mancera Piña P. E. et al., 2019, ApJ, 883, L33
Mancera Piña P. E., Fraternali F., Oosterloo T., Adams E. A. K., Oman K. A., Leisman L., 2022, MNRAS, 512, 3230
Martin G. et al., 2019, MNRAS, 485, 796
Martin N. F. et al., 2016, ApJ, 833, 167
Martín-Navarro I. et al., 2019, MNRAS, 484, 3425
Martínez-Delgado D. et al., 2016, AJ, 151, 96
McConnachie A. W., 2012, AJ, 144, 4
Mihos J. C. et al., 2022, ApJ, 924, 87
Miller B. W., Lotz J. M., 2007, ApJ, 670, 1074
Monelli M., Trujillo I., 2019, ApJ, 880, L11
Montes M., Trujillo I., Infante-Sainz R., Monelli M., Borlaff A. S., 2021, ApJ, 919, 56
Morrissey P. et al., 2018, ApJ, 864, 93
Moster B. P., Naab T., White S. D. M., 2013, MNRAS, 428, 3121
Müller O. et al., 2020, A&A, 640, A106
Müller O. et al., 2021, ApJ, 923, 9
Müller O., Jerjen H., Binggeli B., 2018, A&A, 615, A105
Navarro J. F., Frenk C. S., White S. D. M., 1996, ApJ, 462, 563
Papastergis E., Adams E. A. K., Romanowsky A. J., 2017, A&A, 601, L10
Peng E. W., Lim S., 2016, ApJ, 822, L31
Prole D. J. et al., 2019a, MNRAS, 484, 4865

Prole D. J., van der Burg R. F. J., Hilker M., Davies J. I., 2019b, MNRAS, 488, 2143
Read J. I., Agertz O., Collins M. L. M., 2016, MNRAS, 459, 2573
Román J., Beasley M. A., Ruiz-Lara T., Valls-Gabaud D., 2019, MNRAS, 486, 823
Román J., Trujillo I., 2017a, MNRAS, 468, 703
Román J., Trujillo I., 2017b, MNRAS, 468, 4039
Rong Y., Guo Q., Gao L., Liao S., Xie L., Puzia T. H., Sun S., Pan J., 2017, MNRAS, 470, 4231
Ruiz-Lara T. et al., 2018, MNRAS, 478, 2034
Saifollahi T., Trujillo I., Beasley M. A., Peletier R. F., Knapen J. H., 2021, MNRAS, 502, 5921
Saifollahi T., Zaritsky D., Trujillo I., Peletier R. F., Knapen J. H., Amorisco N., Beasley M. A., Donnerstein R., 2022, MNRAS, 511, 4633
Sales L. V., Navarro J. F., Peñafiel L., Peng E. W., Lim S., Hernquist L., 2020, MNRAS, 494, 1848
Sandage A., Binggeli B., 1984, AJ, 89, 919
Shen Z. et al., 2021, ApJ, 914, L12
Somalwar J. J., Greene J. E., Greco J. P., Huang S., Beaton R. L., Goulding A. D., Lancaster L., 2020, ApJ, 902, 45
Spitler L. R., Forbes D. A., 2009, MNRAS, 392, L1
Tollerud E. J., Bullock J. S., Graves G. J., Wolf J., 2011, ApJ, 726, 108
Tollerud E., 2015, available at: https://gist.github.com/eteq/5000843
Toloba E. et al., 2018, ApJ, 856, L31
Toloba E., Boselli A., Peletier R. F., Falcón-Barroso J., van de Ven G., Gorgas J., 2012, A&A, 548, A78
Torrealba G. et al., 2019, MNRAS, 488, 2743
Tremmel M., Wright A. C., Brooks A. M., Munshi F., Nagai D., Quinn T. R., 2020, MNRAS, 497, 2786
Trujillo I. et al., 2019, MNRAS, 486, 1192
Trujillo-Gomez S., Kruijssen J. M. D., Reina-Campos M., 2022, MNRAS, 510, 3356
van der Burg R. F. J. et al., 2017, A&A, 607, A79
van Dokkum P. et al., 2016, ApJ, 828, L6
van Dokkum P. et al., 2017, ApJ, 844, L11
van Dokkum P. et al., 2018a, Nature, 555, 629
van Dokkum P. et al., 2018b, ApJ, 856, L30
van Dokkum P. et al., 2019, ApJ, 880, 91
van Dokkum P. et al., 2022, Nature, 605, 435
van Dokkum P. G., Abraham R., Merritt A., Zhang J., Geha M., Conroy C., 2015, ApJ, 798, L45
Van Nest J. D., Munshi F., Wright A. C., Tremmel M., Brooks A. M., Nagai D., Quinn T., 2022, ApJ, 926, 92
van Zee L., Skillman E. D., Haynes M. P., 2004, AJ, 128, 121
Villaume A. et al., 2022, ApJ, 924, 32
Willmer C. N. A., 2018a, ApJS, 236, 47
Willmer C. N. A., 2018b, ApJS, 236, 47
Wolf J., Martinez G. D., Bullock J. S., Kaplinghat M., Geha M., Muñoz R. R., Simon J. D., Avedo F. F., 2010, MNRAS, 406, 1220
Wright A. C., Tremmel M., Brooks A. M., Munshi F., Nagai D., Sharma R. S., Quinn T. R., 2021, MNRAS, 502, 5370
Yagi M., Koda J., Komiyama Y., Yamanoi H., 2016, ApJS, 225, 11
Zaritsky D. et al., 2019, ApJS, 240, 1
Zaritsky D., 2017, MNRAS, 464, L110
Zaritsky D., 2022, MNRAS, 513, 2609
Zaritsky D., Donnerstein R., Karunakaran A., Barbosa C. E., Dey A., Kadowaki J., Spekkens K., Zhang H., 2021, ApJS, 257, 60
Zaritsky D., Gonzalez A. H., Zabludoff A. I., 2006, ApJ, 638, 725

APPENDIX: LITERATURE UDG DATA

In this appendix, we present the literature sample of spectroscopically analysed UDGs used in Section 4. Lettering in the notes below corresponds to the superscripts in Table A1.

A0.1 Y358

Notes: a = Calculated from the absolute magnitude assuming $M_\star/L_V = 2$ and $M_{\odot,V} = 4.8$ (Willmer 2018b). b = Circularized

Table A1. Rows from left to right are: (1) Name, (2) Environment {Name}, (3) Distance - although note this is frequently the assumed distance, (4) V-band absolute magnitude, (5) Average V-band surface brightness within the half-light radius, (6) Stellar mass, (7) 2D circularized half-light radius, (8) Recessional velocity, (9) Velocity dispersion from stars or GCs, and (10) GC system number. When relevant errors are given in (brackets) after values. Values unknown are indicated with a '-'. Notes on data are included with superscript letters.

Name	Env.	D (Mpc)	M_V (mag)	$\langle\mu_V\rangle_e$ (mag arcsec^{-2})	$M_\star$ ($\times 10^8$ M$_\odot$)	R_e (kpc)	V_R (km s^{-1})	σ (km s^{-1})	N_{GC}
Y358	Cluster {Coma}	100	−14.8	25.6	1.38[a]	2.1[b]	7969 (2)	19 (3)	28 (5.3)
VCC 1287[a]	Cluster {Virgo}	16.5	−15.6	25.71[b]	2	3.3	1116 (2)	19 (6)	22 (8)
DGSAT I	Field?[a]	78	−16.3	25.6[b]	4	4.4[c]	5439 (8)	56 (10)	12 (2)[d]
Dragonfly 44	Cluster?[a] {Coma}	100	−16.2	25.7[b]	3	3.9	6324[c]	33 (3)	76 (18)[d, e]
DFX1	Cluster {Coma}	100	−15.8	25.5[a]	3.4	2.8	8107[b]	30 (7)[c]	63 (17)
NGC 5846_UDG1[a]	Group {NGC 5846}	26.5	−15.0	25.2[b]	1.1	2.14	2167 (2)[c]	17 (2)[c]	54 (9)[d]
VLSB-B[a]	Cluster {Virgo}	16.5	−13.5[b]	27.5	0.06	2.6[c]	24.9 ($^{+22.3}_{-36.2}$)	47 (+ 53, -29)[d]	26.1 (9.9)
VLSB-D[a]	Cluster {Virgo}	16.5	−16.2[b]	27.6	0.79	9.0[c]	1033.8 ($^{+5.9}_{-5.5}$)	16 (+ 6, -4)[d]	13 (6.9)
VCC 615[a]	Cluster {Virgo}	17.7	−14.7[b]	25.8	0.21	2.3[c]	2094.0 ($^{+14.9}_{-13.0}$)	32 (+ 17, -10)[d]	30.3 (9.6)
UDG1137 + 16[a]	Group {UGC 6594}	21.1	−14.65[b]	26.55[b, c]	1.4	3.3	1014 (3)	15 (4)	-
PUDG-R15	Cluster {Perseus}	75	−15.65[a]	24.83[a]	2.59	2.46[b]	4762 (2)	10 (4)	-
PUDG-R16	Cluster {Perseus}	75	−15.9[a]	25.4[a]	5.75	3.51[b]	4679 (2)	12 (3)	-
PUDG-S74	Cluster {Perseus}	75	−16.49[a]	24.82[a]	7.85	3.52[b]	6215 (2)	22 (2)	-
PUDG-R84	Cluster {Perseus}	75	−15.4[a]	24.68[a]	2.20	1.97[b]	4039 (2)	19 (3)	-
NGC1052-DF2[a]	Group {NGC 1052}[b]	22.1 (1.2)[b]	−15.3	24.8[c]	2	2	1805 (1.1)[d]	8.5 (+ 2.3, -3.1)[d]	7.1 (+ 7.33, -4.34)[e]
Sagittarius dSph	Group {Local}	0.02	−15.5	25.13[a]	1.32	2.6	140 (2)	11.4 (0.7)	8
Andromeda XIX	Group {Local}	0.93	−10	∼ 31[a]	0.0079	3.1	-109 (1.6)	7.8 (+ 1.7, -1.5)	-
Antlia II	Group {Local}	0.132	−9.03[a]	∼ 31.9[b]	0.0088	2.9	290.7 (1.5)	5.71 (1.08)	-
WLM	Group {Local}	0.93[a]	−14.25[b]	26.16[c]	0.41[d]	2.34	-130 (1)	17.5 (2)	1
J125929.89 + 274303.0	Cluster {Coma}	100	−14.88 [a]	25.17 [a]	1.12	2.1	4928 (4)	21 (7)	-
J130026.26 + 272735.2	Cluster {Coma}	100	−16.27 [a]	24.83 [a]	1.56	3.7	6939 (2)	19 (5)	-

using literature *b*/*a* (0.83; van Dokkum et al. 2017). Data sources: This work, van Dokkum et al. (2017), and Lim et al. (2018).

A0.2 VCC 1287

Notes: a = This galaxy is identified as NGVSUDG-14 in Lim et al. (2020). *b* = It is unclear which filter band this is in, although *g*-band seems likely from the context. We therefore transform it into *V*-band using $V = g - 0.3$. Data sources: Beasley et al. (2016), Gannon et al. (2020, 2021), and Lim et al. (2020).

A0.3 DGSAT I

Notes: a = It is located in the Pisces–Perseus supercluster and could potentially be a 'backsplash' galaxy (Martínez-Delgado et al. 2016; Papastergis, Adams & Romanowsky 2017). *b* = Calculated using the properties listed in table 2 of Martínez-Delgado et al. (2016) and equation 11 of Graham & Driver (2005). *c* = Circularized using literature *b*/*a*. *d* = Note that some of these GC's may be overluminous (Janssens et al. 2022). Data sources: Martínez-Delgado et al. (2016), Martín-Navarro et al. (2019), and Janssens et al. (2022).

A0.4 Dragonfly 44

Notes: a = Although in the direction of the Coma cluster, 'it is unclear whether Dragonfly 44 is in a cold clump that is falling into the cluster, a filament, or a structure that is unrelated to Coma' (van Dokkum et al. 2019). *b* = Calculated using the properties listed in table 1 of van Dokkum et al. (2017) at a distance of 100 Mpc and equation 11 of Graham & Driver (2005). *c* = Converted using $V_R = c \times \ln 1 + z$ from the redshift listed in footnote 6 of van Dokkum et al. (2017). *d* = Note the N_{GC} quoted in the abstract is slightly different to this value. Here, we use the value from table 1 of van Dokkum et al. (2017). *e* = Although see Saifollahi et al. (2021) for a differing view of the GC richness of Dragonfly 44. Data sources: van Dokkum et al. (2016, 2017, 2019) and Gannon et al. (2021).

A0.5 DFX1

Notes: a = Calculated using the properties listed in table 1 of van Dokkum et al. (2017) at a distance of 100 Mpc and equation 11 of Graham & Driver (2005). *b* = Converted using $V_R = c \times \ln 1 + z$ from the redshift listed in section 2.1 of van Dokkum et al. (2017). *c* = It is unclear if this is also effected by the barycentric correction issue described in footnote 16 of van Dokkum et al. (2019). Data sources: van Dokkum et al. (2017), and Gannon et al. (2021).

A0.6 NGC 5846_UDG1

Notes: a = This galaxy is referred to as MATLAS-2019 in the MATLAS dwarf galaxy catalog (Habas et al. 2020; Müller et al. 2020, 2021). *b* = Calculated using the properties listed in table 1 of Forbes et al. (2019) and equation 11 of Graham & Driver (2005). Transformed from *g*-band using $V = g - 0.3$. *c* = We prefer these values over those reported in Müller et al. (2020) due to the greater instrumental resolution of Keck/KCWI over VLT/MUSE. *d* = We prefer these values over those reported in Müller et al. (2021) due to the deeper *HST* data used. Data sources: Müller et al. (2020, 2021), Forbes et al. (2021), and Danieli et al. (2022).

A0.7 VLSB-B

Notes: a = This galaxy is identified as NGVSUDG-11 in Lim et al. (2020). *b* = Vega magnitude. *c* = Circularized using literature ellipticity. *d* = This is a GC system velocity dispersion that we assume is equivalent to the stellar velocity dispersion of the galaxy based on the evidence for this assumption in Forbes et al. (2021). Data sources: Toloba et al. (2018) and Lim et al. (2020).

A0.8 VLSB-D

Notes: VLSB-D has an elongated structure and velocity gradient (Toloba et al. 2018) that suggests it is undergoing tidal stripping. *a* = This galaxy is identified as NGVSUDG-04 in Lim et al. (2020). *b* = Vega magnitude. *c* = Circularized using literature ellipticity. *d* = This is a GC system velocity dispersion that we assume is equivalent to the stellar velocity dispersion of the galaxy based on the evidence for this assumption in Forbes et al. (2021). Data sources: Toloba et al. (2018) and Lim et al. (2020)

A0.9 VCC 615

Notes: a = This galaxy is identified as NGVSUDG-A04 in Lim et al. (2020). *b* = Vega magnitude. *c* = Circularized using literature ellipticity. *d* = This is a GC system velocity dispersion that we assume is equivalent to the stellar velocity dispersion of the galaxy based on the evidence for this assumption in Forbes et al. (2021). Data sources: Toloba et al. (2018), Lim et al. (2020), and Mihos et al. (2022).

A0.10 UDG1137 + 16

Notes: UDG1137 + 16 has a disturbed morphology, making it likely it is undergoing stripping (Gannon et al. 2021). *a* = See also Müller et al. (2018) who refer to this galaxy as 'dw1137 + 16'. Transformed to *V*-band using stated $g - r$ colour and $V = g - 0.3$. *c* = Calculated using the properties listed for the single Sérsic fit in table 1 of Gannon et al. (2021) and equation 11 of Graham & Driver (2005). Data source: Gannon et al. (2021).

A0.11 PUDG-R15

Notes: a = Transformed from *g*-band using $V = g - 0.3$. *b* = Circularized using literature *b*/*a*. Data source: Gannon et al. (2022).

A0.12 PUDG-R16

Notes: a = Transformed from *g*-band using $V = g - 0.3$. *b* = Circularized using literature *b*/*a*. Data source: Gannon et al. (2022).

A0.13 PUDG-S74

Notes: a = Transformed from *g*-band using $V = g - 0.3$. *b* = Circularized using literature *b*/*a*. Data source: Gannon et al. (2022).

A0.14 PUDG-R84

Notes: a = Transformed from g-band using $V = g - 0.3$. b = Circularized using literature b/a. Data source: Gannon et al. (2022).

A0.15 NGC 1052-DF2

Notes: This galaxy has both an anomalous star cluster system (van Dokkum et al. 2018b; Shen et al. 2021) and an abnormally low velocity dispersion (van Dokkum et al. 2018a; Danieli et al. 2019). There is also evidence it may be undergoing a tidal interaction (Keim et al. 2022, although see Montes et al. 2021). We do, however, note there is some evidence for rotation in NGC 1052-DF2, which may help alleviate the paucity of dark matter implied by its low velocity dispersion (Lewis, Brewer & Wan 2020; Montes et al. 2021). a = This is also catalogued as [KKS2000]04 in Karachentsev et al. (2000). b = While there existed some initial controversy over the distance of NGC 1052-DF2 (see e.g. Trujillo et al. 2019; Monelli & Trujillo 2019), we believe the deeper data reported in Shen et al. (2021) resolved this issue. We note, however, despite an established distance this does not fully establish an environmental association for NGC 1052-DF2 (see e.g. fig. 5 of Shen et al. 2021). The possibility exists that NGC 1052-DF2 was part of the NGC 1052 group but now resides outside of the group as a consequence of its formation (e.g. van Dokkum et al. 2022). c = Calculated using the properties listed for the single Sérsic fit in table 2 of Cohen et al. (2018) and equation 11 of Graham & Driver (2005). d = We prefer these values over those reported in Emsellem et al. (2019) due to the greater instrumental resolution of Keck/KCWI over VLT/MUSE. e = Here, we use the value of GCs in the roughly expected GC luminosity function window, as reported by Shen et al. (2021). This value excludes the brighter sub-population. Data sources: Danieli et al. (2019) and Shen et al. (2021).

A0.16 Sagittarius dSph

Notes: Note this galaxy is known to be tidally disrupting around the Milky Way (Ibata et al. 2001) a = Calculated using the properties listed in table 1 of Forbes et al. (2018) and equation 12 of Graham & Driver (2005). Data sources: McConnachie (2012), Karachentsev et al. (2017), and Forbes et al. (2018).

A0.17 Andromeda XIX

Notes: Note this galaxy is likely affected by tidal processes interacting with the nearby M31 (Collins et al. 2020). a = Calculated using the properties listed in table 3 of Collins et al. (2020) and equation 12 of Graham & Driver (2005). Due to the extremely diffuse nature of this object, this value is highly uncertain. Data sources: Martin et al. (2016), Collins et al. (2020), and Gannon et al. (2021).

A0.18 Antlia II

Notes: Dynamical modelling suggests that a combination of a cored dark matter profile and tidal stripping may explain the properties of this UDG (Torrealba et al. 2019). a = Vega magnitude. b = Due to the extremely faint nature of Antlia II, this value is highly uncertain. Data sources: McConnachie (2012), and Torrealba et al. (2019)

A0.19 WLM

Notes: WLM is gas-rich and undergoing active star formation (Leaman et al. 2009). a = Calculated from given m - M. b = Vega magnitude. c = Calculated using equation 12 of Graham & Driver (2005). d = Calculated from V-band magnitude assuming $M_\star/L_V = 2$. Data sources: McConnachie (2012) and Forbes et al. (2018)

A0.20 J125929.89 + 274303.0

Notes: a = Converted from R-band using $V = R + 0.5$ (based on Virgo dE's; van Zee, Skillman & Haynes 2004) Data sources: Chilingarian et al. (2019) and Gannon et al. (2021).

A0.21 J130026.26 + 272735.2

Notes: a = Converted from R-band using $V = R + 0.5$ (based on Virgo dE's; van Zee et al. 2004) Data sources: Chilingarian et al. (2019) and Gannon et al. (2021).

This paper has been typeset from a TEX/LATEX file prepared by the author.